Southeastern Europe Tunnelling Conference (SETC-2025)
1-3 October 2025, Belgrade, Serbia

DOI: 10.5937/SETC25021D

Modeling of ground support at Kokhav Hayarden Pumped Storage

Branko Damjanac[a], Ehsan Ghazvinian[a] and Zorica Radakovic-Guzina[a]*

[a] ITASCA, Minneapolis, USA; branko@oneitasca.com, eghazvinian@oneitasca.com, zorica@oneitasca.com

Abstract: The stability of the north walls of the Kokhav Hayarden Pumped Storage Plant powerhouse (PH) and transformer hall (TH) caverns was numerically analyzed. To achieve a calibrated model, this study includes a back-analysis of the displacements recorded by the extensometers in the north walls of the PH and TH caverns, as well as the recorded forces for the instrumented tendons and bar anchors in the same walls throughout the excavation of the caverns. The calibrated model is then used to assess the overall safety margin of the caverns' north wall. The factor of safety (FoS), determined by reducing strength parameters of different geological units, was selected as a simple and reasonable measure of the safety margin to failure. The analyses in these studies were conducted using three-dimensional models in the continuum code FLAC3D, a computationally efficient, state-of-the-art numerical code for modeling the deformation and damage of geo-materials. A few relevant discontinuities are explicitly represented in the model. The model was calibrated for the cavern designs in terms of wall geometry, ground support, and geological information by comparing with the monitoring data (extensometers, prisms, and stress cells) at different locations and throughout the entire excavation history, including the final state of the excavation. In addition to deformation and stability of the excavated caverns, the model predicts the loading (forces) in the ground support (tendons and bar anchors), which is explicitly represented as installed during excavation. The FoS of the north walls of the caverns after complete excavation is greater than 1.5. The forces in five of the tendons and bar anchors in the PH are predicted in the model to slightly exceed their allowable working limit in the final stage of excavation, which is not a concern because the current force measurements for all tendons and bar anchors are within the allowable working limits.

Keywords: pumped storage; powerhouse; excavation stability; tendons; bar anchors; numerical modeling

---

1. Introduction

Kokhav Hayarden (Fig. 1), Israel's largest pumped storage power project, officially began commercial operation on February 21, 2025. Located near the northern Israeli city of Beit She'an, the facility is the lowest-altitude power plant of its kind in the world. The station features an upper reservoir, a water conveyance system, an underground powerhouse (PH), a lower reservoir, and a central building/switchyard. At its core, the underground powerhouse houses two 172-MW reversible hydroelectric generating units, contributing to a total installed capacity of 344 MW. These units play a vital role in enhancing the security and stability of Israel's power grid. The reservoirs have a total capacity of 3.16 million m^3. During peak demand hours, the station will generate electricity by discharging water from the upper reservoir to the lower one and accumulating it by pumping water back into the upper reservoir. The capacity of the new pumped storage power plant will exceed that of the existing hydroelectric power plants in Israel, increasing from the current 306 MW to 650 MW. Solar panels are the primary source of "clean" energy in the country, with their capacity reaching 2.6 GW in 2021.

The PH was excavated in benches, starting with Bench I in the crown. An apparent non-convergent movement was observed for the north wall of the PH after excavation of Bench II exposed the pyroclastic layer on that wall. Installing four pre-tensioned tendons reduced the movement rate, and the wall stabilized further with the installation of an additional three pre-tensioned tendons. After the

*Corresponding author: branko@oneitasca.com (B. Damjanac).

excavation of Bench III was completed, all monitoring data indicated that the north wall had been stabilized.

Fig. 1. An aerial photo of the lower reservoir of Kokhav Hayarden pumped storage power plant.

As the excavations of the PH and adjacent Transformer Hall (TH) continued, the ground support and stability of the excavations were analyzed using a continuously calibrated numerical model. After the excavation of the PH and TH was completed, the monitoring data indicated that the north walls remained stable. The calibrated model was then used to assess the overall safety margin of the north walls of the PH and TH caverns. The factor of safety (FoS), determined by reducing strength parameters of different geological units, was selected as a simple and reasonable measure of the safety margin to failure of the north walls of the caverns. To achieve a calibrated model, this study includes a back-analysis of the displacements recorded by the extensometers in the north walls of the PH and TH caverns, as well as the recorded forces for the instrumented tendons and bar anchors in the same walls throughout the excavation of the PH and TH caverns. Thus, the model is calibrated using all available readings at the end of the excavation, including the tendon and bar anchor forces, as well as displacement information for the north walls. Expansion of the calibration database is crucial for increasing confidence in the calibrated model for FoS assessment.

Hoek (2013) discusses several examples of PH cavern stability and support analyses. The innovative methods for numerical modeling of cavern stability, including efficient and automatic model calibration and sensitivity analyses, are, for example, published by Behnia and Seifabad (2018), Ghorbani and Sharifzadeh (2009), Li et al. (2022), Li et al. (2025), and Zhu et al. (2010). The numerical code FLAC3D (ITASCA, 2019) was used in this study. The preliminary analyses have shown that potential failure mechanisms include failure through the rock mass and sliding on pre-existing structures. A few relevant discontinuities are explicitly represented in the model.

This paper describes the model construction and calibration, as well as input properties used for the numerical analysis, and it provides a summary of the modeling results.

2. Methodology and Model Description

2.1. Model Geometry and Initial Conditions

The three-dimensional model includes the PH and TH caverns as well as the connecting Busbar tunnel between them. The model geometry is shown in Fig. 2. The PH cavern is 82.2 m long, 43 m high, and has a span of 18 m. The cavern axes (y-axis) have orientation N30˚W. Fig. 2 also depicts the lithologies that are explicitly represented in the model. Fault F16, the influence zone of Fault F16—including basalt (bs)-weak Class V (very degraded) material and bs-weak material (above the pyroclastic layer)—as well as the weak pyroclastic layer (Pyr9), are explicitly simulated as zones of finite thickness. Compared to Fault F16, Faults F18 and F22 have a smaller thickness and are not part of the failure mechanism observed in the north wall. Therefore, they are modeled as explicit, discrete features using interfaces (i.e., elements with zero thickness). The preliminary analyses indicate that including a finite thickness for Fault F16 in the model improves the match of the failure mechanism. Ubiquitous joints (i.e., closely spaced fractures) are assumed in the vicinity of the north walls of the PH and TH, where plastic deformation was expected.

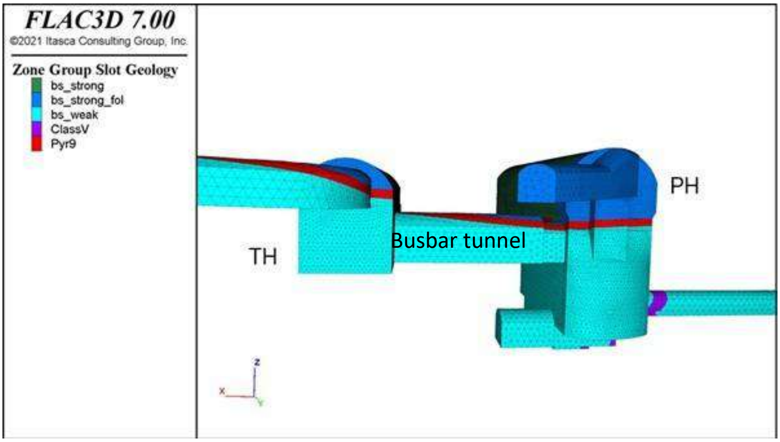

(a)

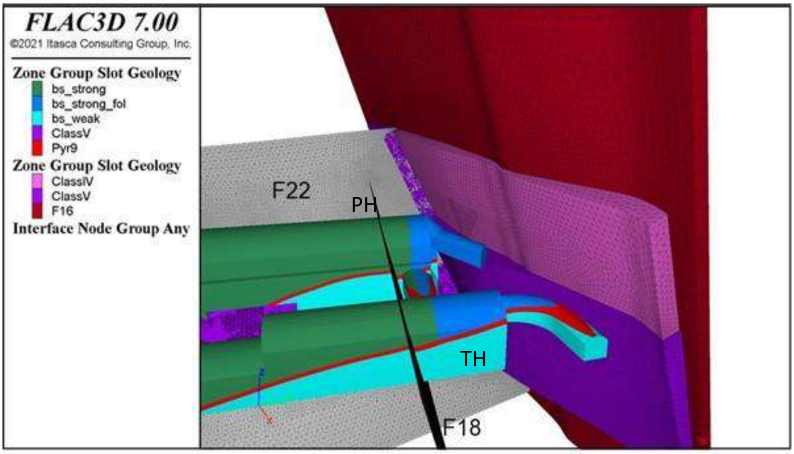

(b)

Fig. 2. (a) Lithologies intersecting the north wall of the PH and TH. (b) Model representation of fault F16, bs-weak Class V material and bs-weak Class IV material (above the pyroclastic layer) in the vicinity of the north wall of the PH and TH.

The in-situ stresses were initialized in the model based on the field measurements. The vertical stress at the PH depth was initialized to 10 MPa (for an approximate depth of 400 m). K_H and K_h of 1.5 and 0.7 were assumed, respectively, with σ_H oriented at N11°W.

The excavation stages are shown in Fig. 3. Note that the excavation of the Busbar tunnel is completed concurrently with the excavation of Bench II and the completion of the excavation of the TH.

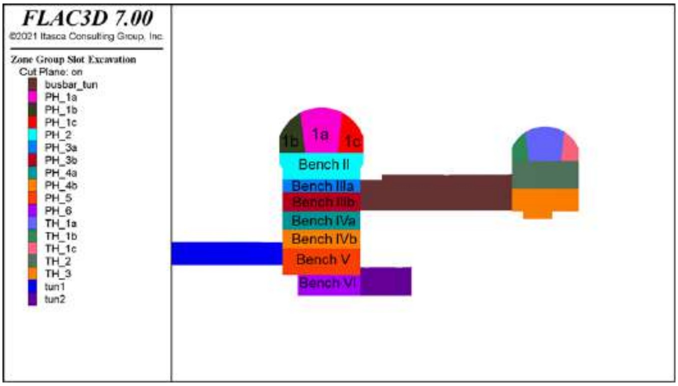

Fig. 3. Excavation stages of the PH.

2.2. Calibrated Rock Mass Properties

The joint set with dip/dip direction of 83°/335°, believed to be the most critical joint set contributing to the wall movement, is represented as ubiquitous joints in the model. The other two joint sets are implicitly represented in the rock mass model, contributing to the calibrated rock mass properties. The volume of the rock mass encompassing the northern section of the caverns (shown in dark blue in Fig. 2) is represented with the SUBI constitutive model, which combines the ubiquitous joints and strain-softening behavior for the rock mass.

The calibrated properties using the observations and monitoring data from the north walls of the caverns are listed in Table 1. The interface properties for F18 and F22 are summarized in Table 2.

Table 1. Rock Mass Properties

Lithology	Constitutive model	E [GPa]	v	UCS [MPa]	Cohesion (residual) [MPa]	Friction angle (residual) [°]	Tensile strength (residual) [MPa]	Critical strain	Dilation angle (residual) [°]
Basalt strong	Strain softening	11.25	0.25	13.7	2.7 (0.1)	47 (47)	0.06 (0.06)	0.03 *[0.014]*	5 (5)
Basalt strong with UB	Subi	11.25	0.25	-	2.7 (0.1) UB: 0.45 (0.05)	47 (47) UB: 31 (31)	0.06 (0.06) UB: 0.0 (0.0)	0.03 *[0.014]* UB: 0.03 *[0.014]*	5 (5) UB: 5 (5)
Basalt weak	Strain softening	7.1	0.25	9.0	2.05 (0.1)	41 (41)	0.03 (0.03)	0.03 *[0.014]*	5 (5)
Faults	Mohr-Coulomb	1.8	0.25	0.3	0.1 (0.1)	23 (23)	0 (0)	-	5 (5)
Pyroclas.	Mohr-Coulomb	1.2	0.25	2.0	0.7 (0.7)	20 (20)	0 (0)	-	5 (5)
Basalt Class V	Mohr-Coulomb	0.97	0.25	2.3	0.76 (0.76)	23 (23)	0 (0)	-	5 (5)

Table 2. Properties Used for F18 and F22 Faults

Contact	Constitutive model	Kn [GPa/m]	Ks [GPa/m]	Cohesion (residual) [MPa]	Friction angle (residual) [°]	Tensile strength (residual) [MPa]
F18 and F22	Coulomb slip	15.0	7.5	0.1 (0)	23 (23)	0 (0)

The strain-softening response is assumed only for the cohesive component of rock mass strengths. The friction angle is assumed to remain constant irrespective of plastic deformation. This is an assumption frequently used in modeling and seems logical from a mechanistic perspective. The damage and plastic deformation create fractures, degrading the cohesive strength of the rock. At the same time, friction is a property of surface contacts and their roughness, and it would not typically decrease with deformation. The discussion of rock mass post-peak behavior and strength softening, including justification of the non-softening frictional behavior, is provided in several publications, such as Kaiser (2019) and Lorig et al. (2020). In any case, the assumption of non-softening friction does not mean that the model is non-conservative, because the model (with constant friction angle, independent of the shear strain and plastic deformation) is calibrated with actual field data and observations.

The calibrated model was able to match the following field observations:

- PH north wall extensometer data.
- Measured forces in the tendons and bar anchors in the north wall throughout the excavation of the PH (this inherently also means matching the wall displacement magnitude).
- The overall deformation of the north wall of the TH.

These comparisons, performed as part of the calibration effort, are discussed in Section 3.

2.3. Ground Support

The typical ground support in the cross-section is shown in Fig. 5(a). The ground support (tendons and bar anchors) designed for the north walls of the PH and TH, in addition to the shotcrete and rock bolts, was installed in the model following the excavation and installation sequences of the caverns.

The additional ground support includes the following:

1. Seven initial tendons (or strand anchors) installed to stop the non-convergent movement that was observed for the north wall after excavation of Bench II. The collar locations of the tendons on the north wall, as represented in the model, are shown in Fig. 4. The tendons are pre-tensioned.
2. Bar anchors that were installed before excavation of Bench III-1, most of which were pretensioned and instrumented with load cells.
3. Additional ground support designed to provide the necessary stability of the north wall and to prevent excessive loads in the previously installed tendons and bar anchors.

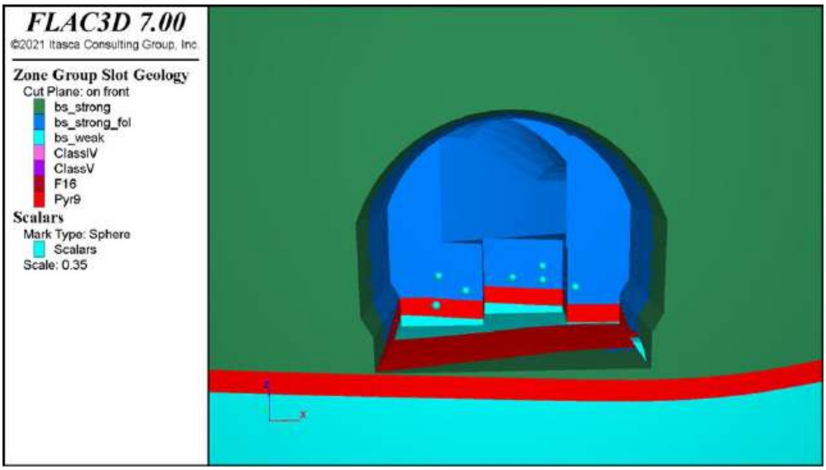

Fig. 4. Collar location of the seven initial tendons in the north wall of the PH.

Fig. 5(b) shows a layout of all the tendons and bar anchors in the north wall of the PH, sidewall, and floor of the adit tunnel in the crown of the PH, installed in addition to the shotcrete and rock bolts at various stages of excavation.

The analysis of the north walls of the PH and the TH includes tendons and bar anchors as the only ground support. Other types of ground support, such as bolts and shotcrete, which do not significantly affect global stability, are not explicitly represented in the model. This approximation is also conservative.

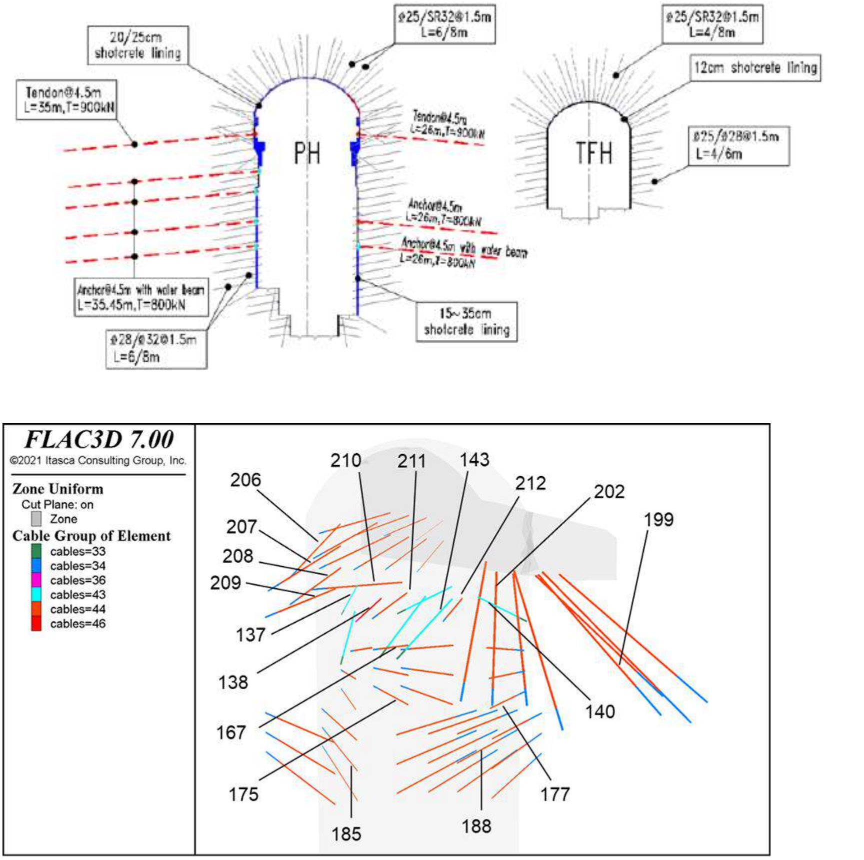

(a)

(b)

Fig. 5. (a) Typical ground support of PH and TH caverns. (b) Layout of the tendons and bar anchors in the north wall of the PH, sidewall, and floor of adit PT1. (The cable element is used to represent both tendons and anchor bars in the model. Colors indicate cable material number, and numbers indicate cable ID for instrumented cables).

In the current model, the tendons and bar anchors behave elastically at forces below their ultimate force capacity, with a subsequent drop to their residual force capacity upon further straining. After softening to residual force, the cables behave as perfectly plastic until reaching the ultimate deformation limit. In the absence of any information regarding the post-failure softening rate for the cables, a brittle response is conservatively considered for the transition from ultimate force capacity to residual force.

Based on the pull-out test in the field, the ultimate force capacity of the tendons was set as 1800 kN in the models, similar to the axial force capacity of the bar anchors. The residual force capacity of the tendons and bar anchors is set to 750 kN. The allowable working force is 900 kN in the tendons and 800 kN in the bar anchors.

3. Model Calibration

Estimation of some rock mass properties (i.e., model input data), including dilation angle, residual friction angle, and critical strain, with limited laboratory and field data and field observations is challenging. Experience and engineering judgment are part of the model calibration procedure. It should be noted that the solution to the calibration process is usually not unique. Multiple sets of properties can potentially satisfy the calibration criteria.

3.1. Extensometer Data from the North Wall of the PH

The displacements measured by the three extensometers installed on the north wall of the PH are shown in Fig. 6. The most important observation from these plots is that the north wall is equilibrated after installation of seven tendons. The depths of the moving ground inferred from the extensometer data are similar to what the model predicts for the same locations (see Fig. 7), which increases confidence in the calibrated model. Note that the goal of the calibration effort was not to exactly match the displacements in the model with those measured by the field extensometers but rather to capture the correct displacement trend and depth of movement in the model.

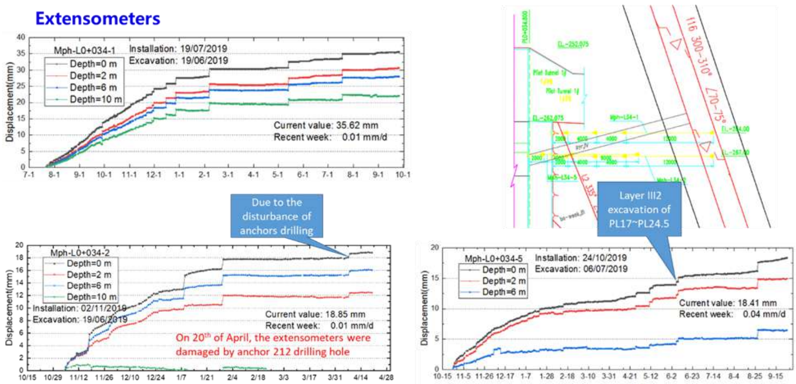

Fig. 6. Displacement data from the extensometers in the north wall of the PH.

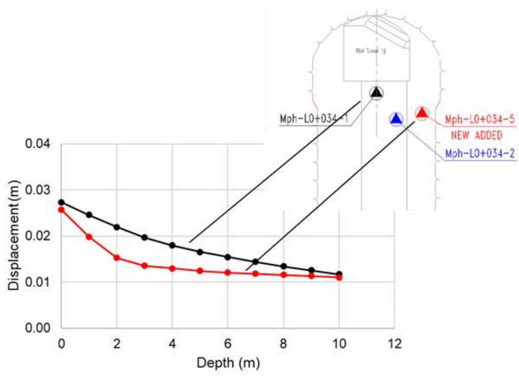

Fig. 7. Displacement data from the numerical model at approximate locations of extensometers in the north wall of the PH after excavation of Bench II.

The exact magnitude of displacements measured in the field can differ from those estimated by the model for a multitude of reasons, such as:

- Inability to replicate the exact installation time of the extensometers in the model. The displacements in the model were zeroed after excavation of Bench I; therefore, the displacements reported in Fig. 7 are the model response to excavation of Bench II.
- The extensometers are measuring the displacement of different sections along the hole relative to their anchor points. In contrast, in the model, the absolute values of deformation at different depths in the north wall are reported.

3.2. Load Cell Data

The calculated forces for all tendons and bar anchors in the north wall after complete excavation of the PH are listed in Table 3 and compared to the measured forces at the site (for instrumented tendons and bar anchors). In general, it is observed that the forces calculated by the numerical model are in good agreement with the load cell data. The forces in five (137, 140, 142, 143, and 210) of the tendons and bar anchors in the PH are predicted in the model to slightly exceed their allowable working limit in the final stage of excavation.

Table 3. Comparison of Forces (t) Measured in the Field and Calculated by the Calibrated Model for Tendons and Bar Anchors after Complete Excavation of the PH.

ID #	Measured	Simulated	ID #	Measured	Simulated
137	83	103	197	21	16
138	28	75	199	31	31
140	75	92	202	36	39
142	58	89	206	30	14
143	62	84	207	21	18
167	21	54	208	39	34
175	19	36	209	34	53
177	28	30	210	78	91
185	24	20	211	31	56
188	26	18	212	24	50
190	24	17			

4. Factor of Safety Analyses

Once the model was calibrated to the monitoring data and other field observations, it was used to demonstrate that the north walls of the PH and TH have sufficient overall FoS with respect to a major failure. For permanent excavations, the FoS should be equal to or greater than 1.5.

The FoS analysis was performed by applying the Strength Reduction Factor (SRF) method to both the rock mass and the strength properties of the faults. It was found that reducing the friction angle of the faults, Class V, and the pyroclastic layer below their nominal values as listed in Table 1 caused them to yield under in-situ stress conditions (far from the excavation), which suggests that either the estimated in-situ stress or the properties of those materials as represented in the model are too conservative. It is most likely that the friction angles of 20–23° for those units are underestimated. Therefore, in the FoS analysis, the SRF is not applied to the friction angle of the materials mentioned above because it is physically inconsistent that rock mass yields under in-situ equilibrium stress conditions.

In the FoS calculations, the response of ground support, including tendons and bar anchors, is represented by a realistic force-displacement curve, including the ultimate force and rupture strain or pull-out displacement (when the support can be assumed to carry no load). During FoS calculations, limiting the response of the ground support to a linearly elastic range would be too conservative because that would result in application of FoS twice, i.e., to the response of the ground support and to the overall response of the supported excavation.

A maximum axial displacement criterion of 0.4 m was used to eliminate the cables from the model based on in-situ pull-out tests. The 0.4 m axial displacement threshold accounts for a minimum of 0.1 m elastic deformation in the unbonded portion of the support at its ultimate force capacity and 0.3 m plastic deformation combined in the unbonded steel and grouted portion of the cable (elastic deformation in the grouted length of the cable is conservatively disregarded). This value is a conservative approximation of the overall cable displacement limit before its load-bearing capacity is drastically reduced based on full-scale pull-out tests performed on anchors ranging between 14 m to 29 m in length with 4 m bonded length (Liu et al., 2017). The bonded sections of the anchors studied by Liu et al. (2017) sustained 0.3–0.4 m of movement, while in this study, and conservatively, the elongation of the cables at their head/collar is limited to 0.4 m (which means smaller movements at their bonded portions). A schematic representation of tendon/bar anchor behavior in the model is shown in Fig. 8. (The representation was selected as a good approximation of the field data and as recommended by Liu et al. (2017).) During the pull-out test, tendon #138 was pulled 10 cm at a constant peak force of 1900 kN without rupture.

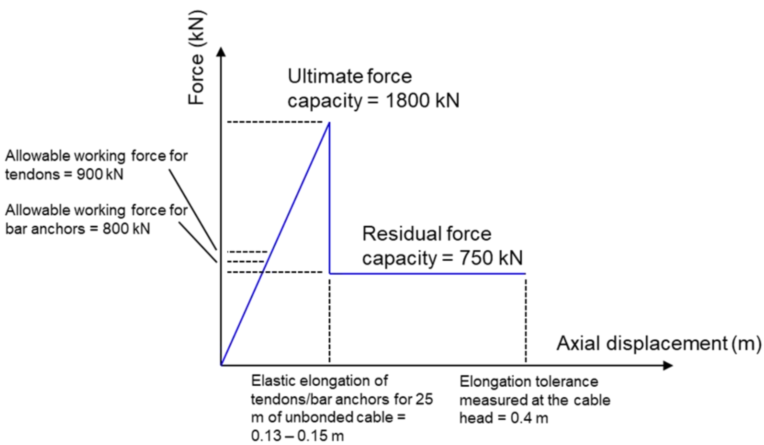

Fig. 8. A schematic representation of tendon/bar anchor behavior in the model.

For FoS analysis, a strength reduction factor (SRF) of 1.5 was applied to the model after complete excavation of the PH and TH. The model reaches equilibrium without signs of instability or non-convergent movement for the north walls of both caverns. The calculated axial forces for the support elements are shown in Fig. 9. Only Tendon 141 (with its collar installed in the pyroclastic layer) reaches 1800 kN, the ultimate force capacity for the tendons, which results in reducing its load capacity to a residual level of 750 kN. The results also indicate that the demand for a FoS of 1.5 in terms of axial displacement of the tendons and bar anchors is well within their 0.4 m displacement tolerance (i.e., the elongation tolerance measured at the head/collar).

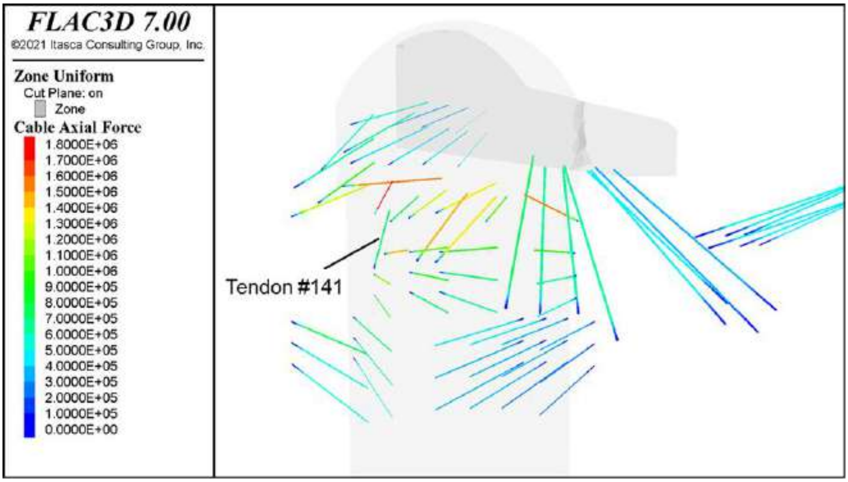

Fig. 9. Contours of axial forces (N) calculated for the support elements after complete excavation of the PH and TH (SRF applied for FoS = 1.5).

5. Conclusion

The detailed model of deformation and stability of the north wall of the PH and TH was developed because of observations of apparent non-convergent deformation in that wall after excavation of Bench II. The seven tendons installed in the north wall of the PH have stabilized it before the excavation of Bench III. The monitoring data indicate that the north wall of the PH remained stable after subsequent excavations, including the final cavern geometry. The additional bar anchors installed on the north wall, as well as the floor and sidewall of the adit tunnel, ensured the required FoS for the final configuration. The calibrated model, in addition to deformation and stability of the excavated cavern, predicts the loading (forces) in the ground support (tendons and bar anchors), which is explicitly represented as installed during excavation. It was also used to evaluate the stability margin expressed by FoS for the north walls of the caverns.

The analysis has shown that the FoS of the north walls of both the PH and TH after complete excavation is greater than 1.5. The forces in five of the tendons and bar anchors in the PH are predicted in the model to slightly exceed their allowable working limit in the final stage of excavation, which is not a concern because the current force measurements for all tendons and bar anchors are within the allowable working limits.

Only one tendon in the PH is predicted to exceed the ultimate force capacity during the FoS calculation. The model reaches equilibrium, and the tendon elongation remains smaller than the pullout tolerance after the force in that tendon is decreased to the residual value.

The conclusions are based on the numerical results. Although a significant effort has been made to calibrate the model to the available field observations, there will always be uncertainties associated with numerical predictions. Monitoring the field response, such as displacements of critical points, and the performance of the installed support, including forces or stresses in the tendons and bar anchors, throughout the operation of the cavern was recommended to ensure that stability conditions do not change.

References

Behnia, M., Seifabad, M.C., 2018. Stability analysis and optimization of the support system of an underground powerhouse cavern considering rock mass variability. *Environ. Earth. Sci.*, 77, pp. 645. https://doi.org/10.1007/s12665-018-7835-2.

Ghorbani, M., Sharifzadeh, M., 2009. Long term stability assessment of Siah Bisheh powerhouse cavern based on displacement back analysis method. *Tunnelling and Underground Space Technology*, 24 (5), pp. 574-583, ISSN 0886-7798, https://doi.org/10.1016/j.tust.2009.02.007.

Hoek, E., 2013. Practical Rock Engineering, Hoek Notes by Evert Hoek. http://www.rocscience.com

Itasca Consulting Group, Inc. (2019) FLAC3D — Fast Lagrangian Analysis of Continua in Three Dimensions (Version 7.0). Minneapolis: Itasca.

Kaiser, P. K., 2019. From common to best practices in underground rock engineering. 8th Mueller lecture presented at the 14th ISRM Congress, Brazil, CRC Press, pp. 141-182.

Li, H., Chen, W., Tan, X., Chen, E., 2022. Digital design and stability simulation for large underground powerhouse caverns with parametric model based on BIM-based framework. *Tunnelling and Underground Space Technology*, 123, pp. 104375, ISSN 0886-7798, https://doi.org/10.1016/j.tust.2022.104375.

Li, H., Chen, W., Tan, X., Wang, X., 2025. Spatial and temporal stability analysis and assessment of underground powerhouse caverns: A case study. *Environ. Earth Sci*., 84, pp. 146. https://doi.org/10.1007/s12665-025-12157-9.

Liu, X., Wang, J., Huang, J., Jiang, H., 2017. Full-scale pullout tests and analyses of ground anchors in rocks under ultimate load conditions. *Engineering Geology*, 228, pp. 1-10.

Lorig, L., Potyondy, D., Varun, 2020. Quantifying Excavation-Induced Rock Mass Damage in Large Open Pits. in Proceedings, 2020 International Symposium on Slope Stability in Open Pit Mining and Civil Engineering (Virtual Conference, May 2020), pp. 969–982. Perth: Australian Centre for Geomechanics.

Zhu, W.S., Li, X.J., Zhang, Q.B., Zheng, W.H., Xin, X.L., Sun, A.H., Li,S.C., 2010. A study on sidewall displacement prediction and stability evaluations for large underground power station caverns. *International Journal of Rock Mechanics and Mining Sciences*, *47*(7), pp 1055-1062, ISSN 1365-1609, https://doi.org/10.1016/j.ijrmms.2010.07.008.